Permeability of Single Nuclear Pores

Oliver Keminer and Reiner Peters

Institut für Medizinische Physik und Biophysik, Universität Münster, D-48149 Münster, Germany

ABSTRACT   In this first application of optical single transporter recording (OSTR), a recently established technique for optically monitoring the activity of single transporters in membrane patches (Tschödrich-Rotter and Peters. 1998. *J. Microsc.* 192:114–125), the passive permeability of the nuclear pore complex (NPC) was measured for a homologous series of hydrophilic probe molecules. Nuclei were isolated from *Xenopus* oocytes and firmly attached to filters containing small cylindrical pores. Transport through membrane patches spanning filter pores was measured by scanning microphotolysis. Thus the permeability coefficients of single NPCs were determined for fluorescently labeled dextrans of ~4, 10, and 20 kDa. Dextrans of ≥40 kDa could not permeate the NPC. The data were consistent with a model in which the NPC contains a single diffusion channel. By application of established theories for the restricted diffusion through small pores, the diffusion channel was approximated as a cylinder with a radius of 4.4–6.1 nm (mean 5.35 nm). Because the transport rate constant of the single NPC was known, the equivalent length of the channel could be also determined and was found to be 40–50 nm (mean 44.5 nm). The symmetry of the NPC implies that a singular component such as the diffusion channel is located at the center of the NPC. Therefore a common transport pathway apparently mediates both passive and signal-dependent transport. To test this hypothesis, measurements of signal-dependent transport and of the mutual effects signal-dependent and passive transport may exert on each other are in progress.

INTRODUCTION

The nuclear pore complex (NPC), a large (Reichelt et al., 1990) and highly differentiated (Akey, 1995; Panté and Aebi, 1996) macromolecular assembly spanning the nuclear envelope, mediates the exchange of matter between the genetic material in the cell nucleus and the protein-synthetizing apparatus in the cytoplasm and thus assumes an important role in cell function and regulation. As a transporter the NPC displays an extraordinary versatility. It has a passive permeability for molecules up to ~5-nm radius (Paine et al., 1975, Peters, 1984) and, in addition, transports larger molecules in a signal-dependent manner (Dingwall et al., 1982; Kalderon et al., 1984; Wen et al., 1995; Fisher et al., 1995). Signal-dependent transport is bidirectionally selective in the sense that certain substances are only imported, others only exported, and still others shuttle (Goldstein, 1958; Borer et al., 1989; Meier and Blobel, 1992; Michael et al., 1995).

The biochemical and molecular genetic characterization of nuclear transport has experienced a remarkable progress in recent years (for review, see Melchior and Gerace, 1995; Nigg, 1997; Pemberton et al., 1998; Mattaj and Englmeier, 1998; Görlich, 1998). Thus the knowledge about import signals (nuclear localization signals, NLS) has been expanded, and export signals (nuclear export signals, NES) have been newly identified. Soluble carriers referred to as karyopherins or as importins/exportins, which bind NLS- or NES-containing proteins and carry them through the NPC, have been characterized and found to comprise a whole familiy of analogous proteins. The small G-protein Ran was found (Moore and Blobel, 1993) to be an essential transport factor, and it is now widely believed (Cole and Hammill, 1998) that its GDP/GTP cycle is the clue to directional selectivity.

Despite this progress, however, the molecular mechanisms underlying the actual transport process have remained largely elusive. For the signal-dependent import some major steps could be discriminated: binding of a NLS-containing substrate to karyopherin/importin, docking of the complex at the cytoplasmic filaments of the NPC, migration or transport of the complex to the central transporter of the NPC, translocation of the complex through the transporter, and eventually the release of the complex and its dissociation in the nucleus. For the simplest transport mode, passive diffusion, essentially two mechanisms are being discussed. Thus, according to one model (Hinshaw et al., 1992), the NPC contains eight diffusion channels (DCs) positioned symmetrically around the NPC center at a perimeter of ~50 nm. In contrast, recent studies (Feldherr and Akin, 1997) strongly suggest that there is only a single DC traversing the center of the NPC.

In a long-range effort comprising six major steps (Peters et al., 1974, 1990; Peters, 1983; Wedekind et al., 1994; Tschödrich-Rotter et al., 1996; Tschödrich-Rotter and Peters, 1998), we have developed a method, optical single transporter recording (OSTR), for optically recording the activity of single transporters in membrane patches. Cells or organelles are firmly attached to isoporous filters, and the transport across membrane patches spanning filter pores is measured by confocal laser scanning microphotolysis (SCAMP) (Wedekind et al., 1994), the amalgamation of

---

microphotolysis and laser scanning microscopy. Combining fluorescence detection, photochemical activation, and a novel membrane patching technique, OSTR is characterized by 1) a high specificity permitting simultaneous monitoring of two or more transport substrates; 2) an extremely high sensitivity extendable to the single-molecule level that permits monitoring of all types of membrane transporters, including those with small transport rates such as carriers and pumps; 3) a time resolution that can be extended to the millisecond range by employing the line scanning mode of the confocal microscope (Wedekind et al., 1996); 4) the possibility of modulating substrate or cofactor (e.g., ATP) concentrations by photobleaching or photoactivation; 5) the ability to freely chose the size of membrane patches within wide limits (0.1–10.0 μm diameter), allowing the adjustment of the patch size to the transporter density and monitoring of single transporters (small patches) or defined populations of transporters (larger patches); 6) the ability to monitor up to 100 membrane patches in parallel; 7) in the case of the nuclear envelope of *Xenopus* oocytes and potentially other membrane systems, the ability to freely and independently adjust the media on the two sides; 8) in the case of energy-dependent transporters, the ability to start transport by the addition of ATP, thus perfectly avoiding a photolysis step.

After OSTR was established using particularly simple biological systems (cytolytic pores in erythrocyte membranes; Peters et al., 1990; Tschödrich-Rotter et al., 1996; Tschödrich-Rotter and Peters, 1998), it was applied in the present study for the first time to a cell biologically important and currently intensively studied topic, nucleocytoplasmic transport. For the purpose here the method was further refined and adopted to measurements of transport through single NPCs. It turned out that the nuclear envelope of *Xenopus* oocytes is a much "easier" object for OSTR than the erythrocyte membrane. Thus, in the case of erythrocytes, the seal between cell membrane and isoporous filter, a critical parameter of OSTR, was only tight for dextrans $\geq$40 kDa, corresponding to a Stokes radius of approximately $\geq$4.5 nm. Even this relatively loose seal could be only achieved by a brief treatment with polyethylene glycol. In contrast, in the case of the nuclear envelope, the tightness of the seal apparently extended, without polyethylene glycol treatment, down to probe molecules of 2.5 nm Stokes radius.

Thus the permeability coefficients of single NPCs for dextrans of ~4, 10, or 20 kDa were determined. The results showed that the NPC contains only a single DC. Its dimensions are equivalent to those of a cylindrical pore of ~5-nm radius and 45-nm length. Taking the radial symmetry of the NPC into account, a singular component such as the DC should be located in the center of the NPC. This implies that passive and signal-dependent transport are mediated by a common channel. The expected interference between passive and signal-dependent transport is currently under study.

EXPERIMENTAL PROCEDURES

Materials

The fluorescein-labeled dextrans FD4 (mean molecular mass 3.9 kDa) and FD20 (mean molecular mass 17.2 kDa) were obtained from Sigma (Deisenhofen, Germany), and FD10 (mean molecular mass 10.0 kDa) was from Molecular Probes Europe (Leiden, The Netherlands). The translational diffusion coefficients of the dextrans were determined by photobleaching, as described previously (Peters, 1984). For transport measurements the dextrans were dissolved at a final concentration of 4 g/liter in a buffer mimicking the intracellular milieu of *Xenopus* oocytes ("oocyte mock buffer") containing 140 mM KCl, 3 mM MgCl$_2$, and 10 mM HEPES (pH 7.2).

Isoporous filters of the type 0.2L (nominal pore diameter 0.2 μm) were obtained from Infiltec (Speyer, Germany), and filters of type 150611 (nominal pore diameter 2.0 μm) were from Nucleopore (Tübingen, Germany). According to the manufacturers, the nominal values of the pore diameters are maximum values, and the actual pore radii vary between a nominal value and nominal value minus 20%. Therefore we assumed a mean pore radius of nominal value minus 10%. Before use, pieces of ~1 cm × ~1 cm were cut from the filters and immersed overnight in a solution of poly-D-lysine, molecular mass > 300 kDa (Sigma, Deisenhofen, Germany; final concentration 0.1 g/liter) in distilled water. Immediately before use the filter pieces were carefully washed in distilled water and then immersed in a so-called patch buffer containing 120 mM KCl, 10 mM NaCl, 2 mM MgCl$_2$, 1.1 mM EGTA, and 10 mM HEPES (pH 7.4).

Attachment of nuclei to isoporous filters

Stage VI oocytes were prepared from *Xenopus laevis* according to the method of Smith et al. (1991) and kept for further use in a buffer containing 88 mM NaCl, 1 mM KCl, 0.8 mM MgSO$_4$, 1.4 mM CaCl$_2$, 5 mM HEPES (pH 7.4), as well as 100 U/ml penicillin and 0.1 g/liter streptomycin. Immediately before isolation of nuclei, oocytes were transferred into mock buffer. Nuclei were then isolated manually according to the method of Evans and Kay (1991). Immediately before nuclei were attached to isoporous filters, the nuclei were transferred into patch buffer. A filter piece, coated with polylysine and suspended in patch buffer as described above, was placed on a piece of parafilm. An isolated nucleus was deposited in the center of the filter piece. The filter piece together with the nucleus was then placed on a piece of laboratory tissue that had been wetted with patch buffer. It followed the simple yet important step in which the wet piece of laboratory paper was blotted at its free edges with dry paper, thus inducing a fluid stream through the filter pores and firmly attaching the nucleus to the filter. The further sequence of manipulations is described in detail in the Results and illustrated there in Fig. 1.

### Transport measurements by scanning microphotolysis

Measurements were performed as described (Tschödrich-Rotter and Peters, 1998), employing a Leica TCS 4D confocal laser scanning microscope equipped with a 100-fold, NA 1.3 objective. A single photolysis scan, lasting ~1 s, was sufficient to reduce the fluorescence of the filter pores by ~66%.

Evaluation of transport data

When a passive transport process is measured by OSTR, the time-dependent fluorescence intensity of the filter pore is given by a simple exponential (Tschödrich-Rotter and Peters, 1998):

$$F(t) = F(0) + [F(\infty) - F(0)][1 - e^{-k_n t}] \qquad (1)$$

FIGURE 1 Scheme of the method for functionally isolating small membrane patches containing few nuclear pore complexes. The nuclear envelope was firmly attached to an isoporous filter, i.e., a 10-μm-thick translucent sheet of polycarbonate containing a homogeneous population of cylindrical pores. In a filter type with pores of 0.18 μm diameter, the membrane patches spanning filter pores contained 1.25 nuclear pore complexes on average. Transport through the nuclear pore complexes into the filter pores was measured by scanning microphotolysis, a combination of fluorescence microphotolysis and confocal laser scanning microscopy. Not drawn to scale.
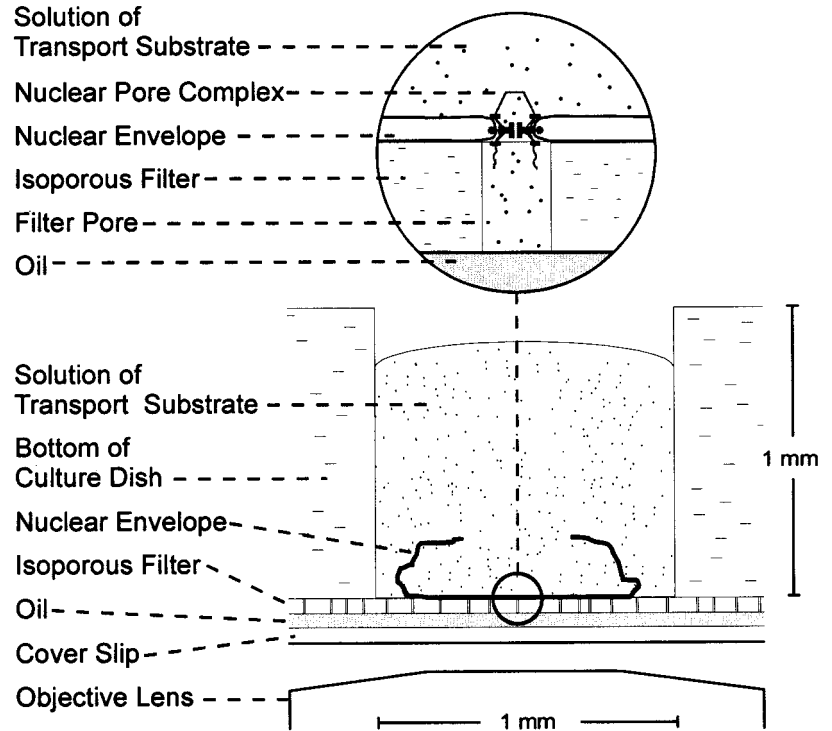
where $F(t)$, $F(0)$ and $F([\infty])$ are background-corrected fluorescence of the filter pore at time t, 0, and ∞; k_n is the transport rate constant of a membrane patch containing n transporters; and t is time after photolysis. The relation between k_n, n, and the intrinsic permeability coefficient P of the single transporter (dimension:volume/time) is

$$k_n = nP/V_{fp} \tag{2}$$

where V_{fp} is the volume of the filter pore. For large membrane patches containing many transporters, $n = sA_{fp}$, where s is the mean area density of transporters and A_{fp} is the cross section of the filter pore. Then, for a cylindrical filter pore, the transport rate constant is given by

$$k_n = sP/l_{fp} \tag{3}$$

where l_{fp} is the length of the filter pore. Equation 3 shows that for large filter pores k_n is independent of the filter pore radius. It follows that the relation between k_n measured with large filter pores and k_1 measured with small filter pores is

$$k_n = sA'_{fp}k_1 \tag{4}$$

where A'_{fp} is the cross section of the small filter pore. k_1 is the rate constant of a membrane patch with one transporter.

The evaluation of the experimental data, including the determination of the time-dependent fluorescence intensities of the filter pores, the fitting of the experimental fluorescence curves by Eq. 1, the generation of frequency diagrams, the smoothing of the frequency diagrams by a mean filter with $n = 7$, and the fitting of the frequency diagrams by a sum of independent Gaussians, was as described (Peters et al., 1990; Tschödrich-Rotter et al., 1996; Tschödrich-Rotter and Peters, 1998).

Calculation of the equivalent dimensions of the diffusion channel

A theoretical framework for the restricted diffusion and flow through small cylindrical pores was developed by the early 1950s (Pappenheimer et al., 1951), later refined (for reviews, see Bean, 1972, and Renkin and Curry,

1979), and frequently applied, also to the NPC (Paine and Scherr, 1975; for a review, see Peters, 1986). Adopted to the present case (Tschödrich-Rotter and Peters, 1998), the effective radius r_{eff} of a cylindrical pore is given by

$$r_{eff} = \sqrt{\frac{k_1 l_{DC} V_{fp}}{\pi D}} \tag{5}$$

where l_{DC} is the length of the diffusion channel and D is the diffusion coefficient of the probe molecule in the diffusion channel. Equation 5 assumes that the molecular radius a of the substrate is much smaller than the geometrical radius r_0 of the pore. For a finite a/r_0 ratio, the steric hindrance at the entrance of the pore and the friction at the pore wall are accounted for by

$$\frac{r_{eff}}{r_0} = \left(1 - \frac{a}{r_0}\right) \bigg/ \sqrt{\kappa_1} \tag{6}$$

where κ_1 is a factor that depends on the a/r_0 ratio and has been tabulated (Paine and Scherr, 1975). The calculation of r_0 according to Eqs. 5 and 6 requires a knowledge of l_{DC}, which, in general, is not available. However, by combining the data of any two transport substrates a and b, l_{DC} can be eliminated and r_0 calculated according to

$$\frac{k_{1a}D_b}{k_{1b}D_a} = \left[\frac{1 - a_a/r_0}{1 - a_b/r_0}\right]^2 \frac{\kappa_{1b}}{\kappa_{1a}} \tag{7}$$

When r_0 has been determined, l_{DC} can be calculated from the data of each probe molecule by

$$l_{DC} = \frac{\pi D(r_0 - a)^2}{\kappa_1 k_1 V_{fp}} \tag{8}$$

Simulation of frequency diagrams

To find out which of the models for the number and arrangement of diffusion channels in the NPC is appropriate, frequency diagrams were

simulated for the models employing principles established previously (for details, see Peters et al., 1990). According to that analysis the probability density of k, i.e., the probability that a given k value occurs within a small k interval, is given by

$$D(k) = \sum_{n} P_n G_n \qquad (9)$$

Here, P_n is the probability that a membrane patch carries n DCs. G_n is a Gaussian of the form

$$G_n = \frac{1}{\sqrt{2\pi}\,\sigma_n} e^{-(1/2)((k-k_n)/\sigma_n)^2} \qquad (10)$$

where σ_n, the standard deviation of the G_n, is determined by

$$\sigma_n = \sigma_0 + n\sigma_1' \qquad (11)$$

σ_0 and σ_1 are the standard deviations of membrane patches with 0 and 1 DC, and k_n, the mean value of G_n, is given by

$$k_n = nk_1 \qquad (12)$$

RESULTS

Adaptation of the patch method to the nuclear envelope

The general structure of samples employed in the present study is indicated in Fig. 1. Sample preparation was begun by placing a small piece of an isoporous filter, which had been coated in advance with polylysine, on a wet sheet of laboratory paper. Then, a cell nucleus, isolated manually from a *Xenopus* oocyte, was placed on the piece of filter. By blotting the wet laboratory paper at its free edges with dry paper, a gentle stream of fluid through the filter was induced. The stream firmly attached the nuclear envelope to the filter and caused the nucleus to burst. Thus the nuclear envelope spread out as a single plane membrane covering the filter over an approximately circular area of 1 mm diameter. The filter pores were then filled with a desired solution ("external medium") and subsequently sealed at their membrane-free openings. These two steps were achieved by placing the piece of filter with its membrane-free surface at first on a drop of "external buffer," deposited on a coverslip, and then on a drop of mineral oil, deposited on another coverslip. The latter, together with the piece of filter, was attached to a "microcuvette." In the present study a microcuvette of ~1–2-mm diameter and 1-mm depth was generated simply by drilling a hole through the bottom of a culture dish. The coverslip was mounted on the bottom of the culture dish such that the nuclear envelope was positioned at the center of the hole. The residual mineral oil on the coverslip surrounding the filter piece caused the coverslip to firmly adhere to the culture dish. The preparation was finished by filling the hole in the culture dish bottom with a desired solution ("internal medium"). Importantly, the procedure permits us to place different media on the cytoplasmic and nuclear sides of the NPC and, in addition, provides free access to the internal medium during measurements.

Prediction of the distribution of nuclear pore complexes among membrane patches

Isoporous filters are thin translucent sheets made of polycarbonate containing homogeneous populations of circular pores. In a preceding study concerning streptolysin O pores in erythrocyte membranes (Tschödrich-Rotter and Peters, 1998), we employed filters with pore diameters of 1–3 μm and adjusted the density of streptolysine O pores appropriately. However, in the case of the NPC, a perfectly different situation was given. In the nuclear envelope of amphibian oocytes, the NPCs are extremely densely packed. For instance, in stage VI oocytes of *Xenopus laevis*, which were used in the present study, the density amounts to ~50 NPC/μm^2 (Maul, 1977), i.e., the area per NPC is ~0.02 μm^2 on average. Therefore, a filter type seemed most appropriate with a pore diameter of 0.18 μm, corresponding to a pore cross section 0.025 μm^2.

To predict the distribution of diffusion channels among membrane patches, we simulated the distribution of NPCs in the oocyte nuclear envelope on the basis of published electron micrographs. In Fig. 2 such an array of NPCs is schematically shown. NPCs are indicated as circles and DCs as dots within the circles. The arrangement of NPCs is identical to that in figure 4 of Franke and Scheer (1974); however, the magnification was scaled down by 10% to obtain a density of 50 NPC/μm^2. Figure 2 *a* is based on a model in which the NPC contains a single central DC. Figure 2 *b* assumes that there are eight diffusion channels per NPC, distributed symmetrically around the center at a radius of 50 nm. Eventually, Fig. 2 *c* assumes that the NPC has one central DC and eight peripheral DCs. The shaded circles in Fig. 2, *a–c*, represent filter pores of 0.18-μm diameter. Their size and density correspond to the filter type (Infiltec GmbH, Speyer, Germany; type 0.2L) we employed in the present measurements. In Fig. 2, *a–c*, a filter pore of 1.8-μm diameter is also indicated (*large circle*). We used such large filter pores in some experiments for comparison.

The distribution of DCs among membrane patches of 0.18-μm diameter was derived by counting, for many randomly distributed filter pores, the number of DCs found inside filter pores. Concerning the effects the intimate contact between NPC and filter may exert on the permeability of the DCs, two possibilities were considered. The first one ("local blockade mode," Fig. a'–c') assumed that the membrane-filter contact only blocks the permeability of DCs in direct contact with the filter. DCs inside the filter pore have a normal permeability, even if they belong to NPCs that are partially in contact with the filter. The second possibility ("global blockade mode," Fig. a''–c'') assumes that, perhaps by long-range conformational changes, the permeability of all DCs of a NPC is blocked whenever a part of that NPC is in contact with the filter, i.e., only DCs were counted which belonged to NPCs that were completely within the filter pore without touching the filter.

It was found that for the local blockade mode and assuming a single DC/NPC (Fig. 2 a'), most membrane patches
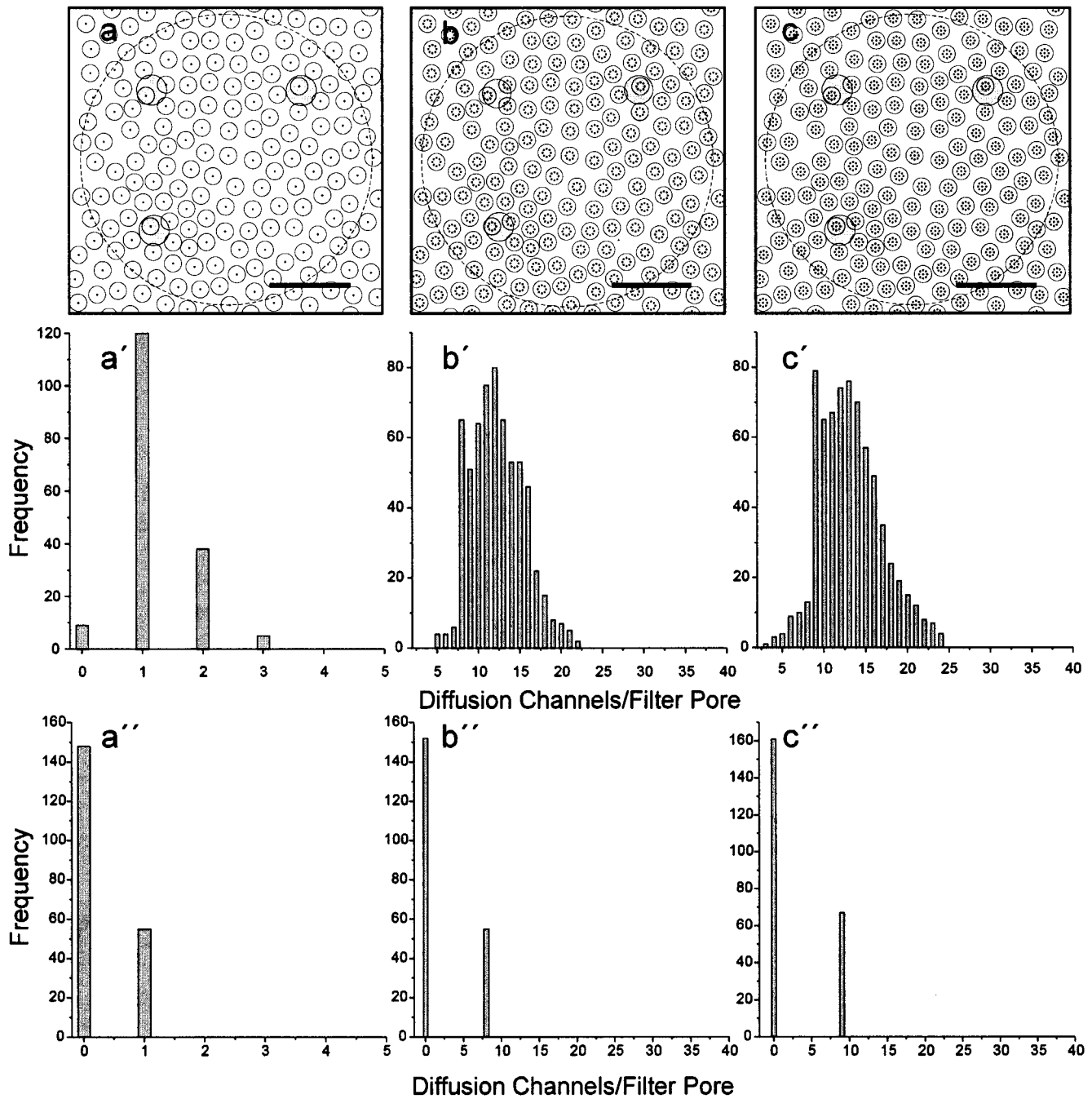
FIGURE 2   Prediction of the distribution of diffusion channels among membrane patches. (a–c) A small part of the nuclear envelope of *Xenopus* oocytes. The nuclear pore complexes are indicated as open circles. Their distribution was adopted from published electron micrographs. Three models for the number and arrangement of diffusion channels of the nuclear pore complex were considered: (a) one central diffusion channel (*dot*) per nuclear pore complex, (b) eight diffusion channels (*dots*) distributed around the center at a perimeter of 50 nm, or (c) one central plus eight peripheral diffusion channels. The shaded circles represent filter pores of 0.18 μm diameter. The large circle represents a filter pore of 1.8 μm diameter. Scale bars, 500 nm. The distribution of diffusion channels among membrane patches of 0.18 μm diameter was predicted by counting the occurrence of diffusion channels within filter pores for a large number of randomly distributed filter pores. In a'–c' it was assumed that in case of a partial contact of a NPC with the filter, the diffusion channels in the free part of the NPC are not closed (local blockade mode). In contrast, a''–c'' assumed that all diffusions channels of a NPC are closed (e.g., by induced conformational changes) whenever the NPC has any contact with the filter (global blockade mode).

contained one channel (~70% of total), whereas the fractions containing no, two, or three channels amounted to ~5%, ~20%, and ~3%, respectively. The peaks corresponding to patches with no, one, two, or three diffusion channels are equidistantly spaced on the abscissa. In contrast, the models assuming eight or nine DCs (Fig. 2, b' and c') yielded broad distributions made up of many closely spaced peaks with an overall maximum at ~12 or 13 DCs

and secondary maxima or shoulders at 8 or 9 and 14 or 16 DCs.

The global blockade mode yields perfectly different distributions (Fig. 2, a''–c''), all of which are characterized by having a large fraction (70–73%) of membrane patches with no open DCs and only a single fraction (27–30%) of permeable membrane patches carrying one, eight, or nine open DCs, depending on the model.

Results of transport measurements

As transport substrates we employed a series of fluorescently labeled dextrans. The samples were made up as described above (Fig. 1), using the same medium on both sides of the nuclear envelope. An example of a measurement in which a filter with 0.18-μm-diameter pores and a 10-kDa dextran were employed is shown in Fig. 3. At first (Fig. 3 a), an array of filter pores was imaged by confocal scanning employing a nonbleaching laser power. The image was used to select a number of filter pores which, by their circular appearance, seemed to traverse the filter perpendicularly. Then, selected filter pores were photobleached at an elevated laser power of $\sim$2.000-fold, employing the SCAMP method (Fig. 3 b). The depletion of the filter pores by fluorescence as well as the restoration of fluorescence by transport of fresh dextrans through the membrane patches spanning the filter pores was followed by repetitive imaging at a nonbleaching laser power (Fig. 3, c–f).

The quantitation of such measurements is illustrated in Fig. 4. The relative fluorescence intensity of individual filter pores was read from the confocal images and plotted versus time (Fig. 4 a, $symbols$). The three phases of the measurement, prephotolysis, photolysis, postphotolysis, can be recognized. The postphotolysis phase was fitted by a single exponential (Fig. 4 b, $line$) according to Eq. 1 to obtain the transport rate constant k_n.

Although dextrans of 4–70 kDa were tried, the NPC was found to be, on the time scale of our experiments, virtually impermeable for dextrans $\geq$ 40 kDa. For each of the permeable dextrans transport was measured employing both 0.18-μm or 1.8-μm filters. About 200–250 measurements were collected for each condition. The results were presented as frequency diagrams, as shown in Fig. 5 and 6. In this type of analysis the number of times a particular transport rate constant occurs within a population of measurements is plotted versus the value of the rate constant.

The frequency diagrams for 0.18-μm filter pores are shown in Fig. 5. For all of the dextrans the experimental values ($bars$) split up into three or four peaks, which were distributed equidistantly on the k-axis and could be fitted by a sum of Gaussians ($lines$). The peak values of the individual Gaussians were taken as mean values of the corresponding rate constants; these are designated as k_0, k_1, k_2, and k_3 and listed in Table 2, together with some relevant properties of the probe molecules.

Frequency diagrams corresponding to experiments employing a filter type with pores of 1.8-μm diameter are
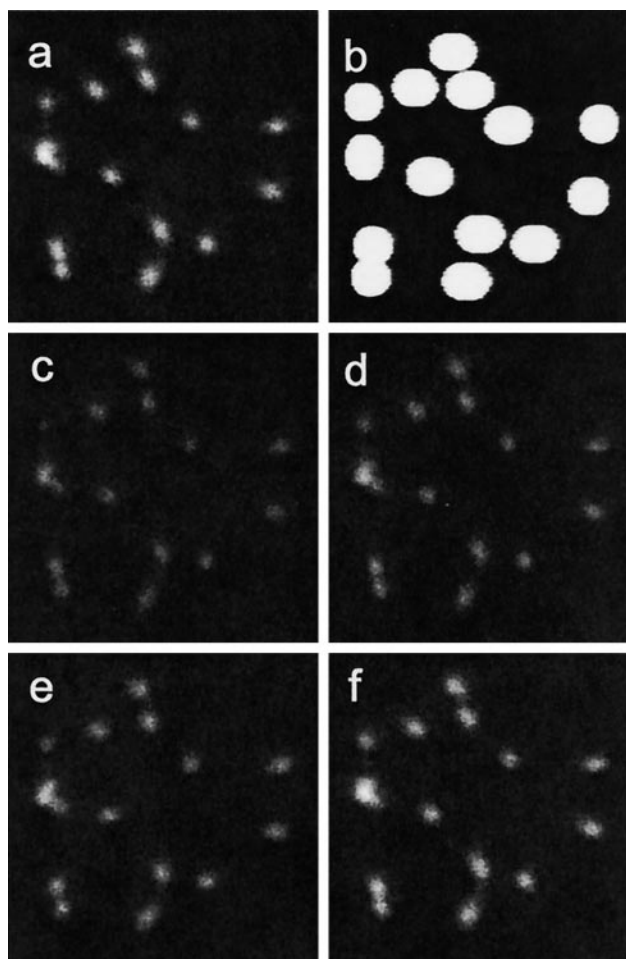

FIGURE 3 Example of an optical single transporter recording. A specimen was prepared according to the scheme of Fig. 1, employing a filter type with pores of 0.18 μm diameter and adding a fluorescently labeled 10-kDa dextran to the solution. (a) Filter pores were visualized by a confocal scan. (b) Several filter pores were photobleached by a scan in which a largely increased laser power was employed, however, with the laser beam switched on only in the selected areas ($bright circles$). (c–f) The depletion of the photolyzed filter pores of fluorescence and the restoration of fluorescence by transport of fresh dextran through the nuclear pore complex into the filter pores was visualized by confocal scans taken (c) immediately, (d) 30 s, (e) 150 s, and (f) 300 s after photolysis.

shown in Fig. 6. The experimental values ($bars$) show a single peak that could be fitted by a single Gaussian ($full line$). This was to be expected, because the membrane patches contained $\sim$125 NPCs, and the measurements yielded an average of the NPC assembly. The peak values of the Gaussians are referred to as k_{125}; these are also listed in Table 1.

Determination of the number of diffusion channels per nuclear pore complex

In the present context the transport rate constant k_n of a membrane patch is directly proportional to the number n of DCs in that patch (Eq. 2). Therefore the frequency distribution of k is directly correlated with that of n, and a
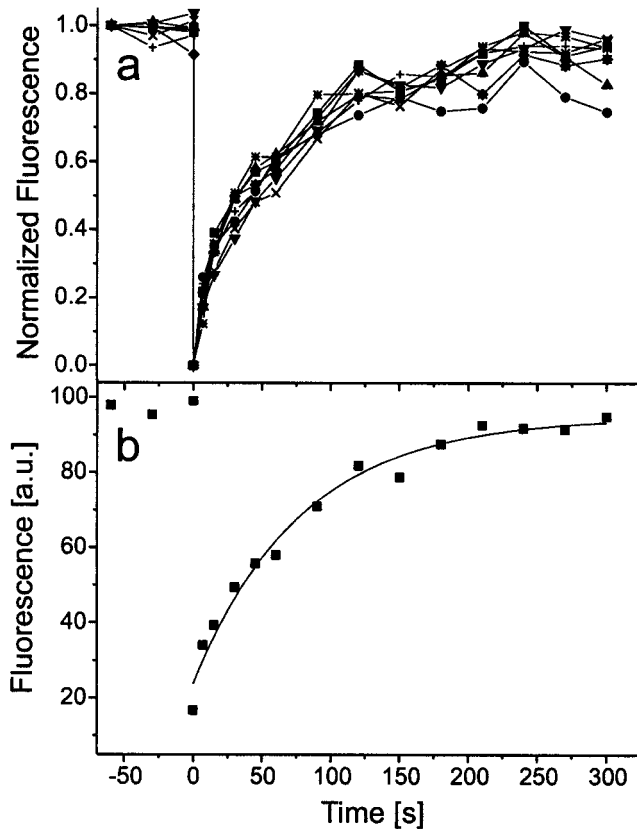
FIGURE 4   Evaluation of optical single transporter recordings. Confocal scans such as those shown in Fig. 3 were evaluated by determining the fluorescence intensity values of the photolyzed filter pores and plotting the values versus time. (*a*) An example for data evaluation corresponding to Fig. 3 is given. (*b*) The time-dependent fluorescence intensity of individual filter pores (*symbols*) was fitted by a simple exponential according to Eq. 1 (*line*) to obtain the transport rate constant.

comparison of experimentally determined k distributions (Fig. 5) with predicted DC distributions (Fig. 2) is highly instructive. Obviously, the experimental distributions (Fig. 5) are only compatible with the frequency distribution of the model assuming one DC per NPC and the local blockade mode (Fig. 2 a'). For both the experimental data and the predicted DC distribution, the frequency diagrams show three or four well-separated and equidistantly spaced peaks of qualitatively similar magnitudes. In contrast, all other predicted DC distributions are not consistent with the experimental data. Thus, if there are eight or nine DCs per NPC, the local blockade mode yields a large number of closely spaced peaks (Fig. 2, b' and c'), whereas the global blockade mode yields, for all three NPC models, a predominant fraction with $n = 0$ (Fig. 2, a''–c''), in definite contradiction to the experimental data, in which the fraction of impermeable patches was very small. This suggests that the NPC contains a single DC and that the local blockade mode is effective.

However, although closely related to each other, the distributions of k and n differ in as much as n has integer values, whereas k has a spread around a mean value. To
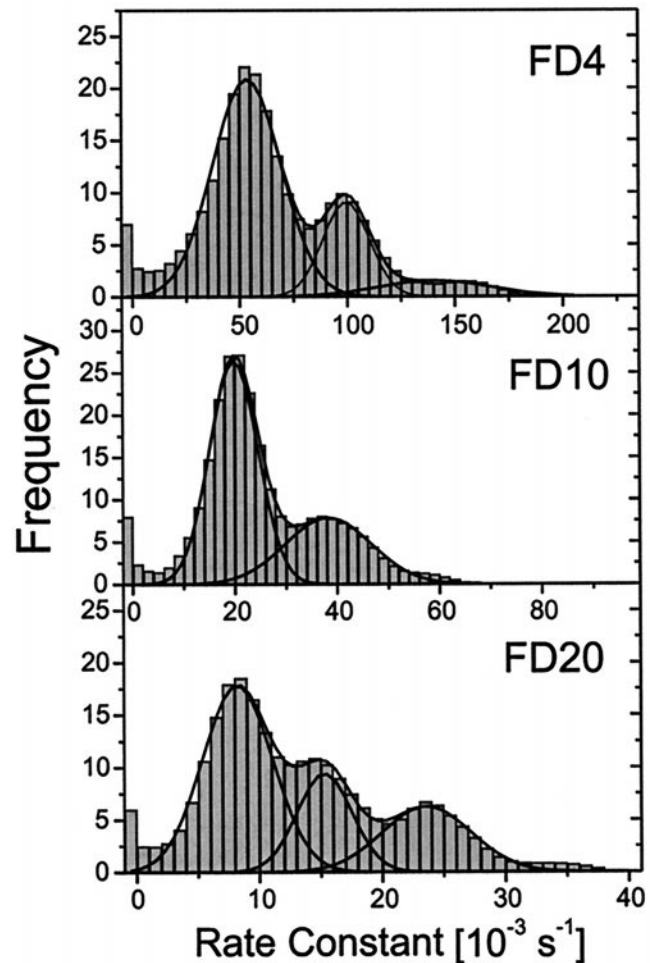

FIGURE 5   Results of measurement concerning small membrane patches. Employing a filter type with pores of 0.18 μm diameter to isolate membrane patches containing 1.25 nuclear pore complexes on average; for each of the probe molecules (FD4, FD10, FD20); ~250 measurements of the transport rate constant were made. The results were plotted as frequency diagrams in which the number of times a particular rate constant occurs in the population is plotted versus the rate constant. For each of the probe molecules the experimental data (*columns*) are seen to split up into distinct peaks, which are equidistantly spaced on the abscissa. For the different probe molecules the rate constants depended inversely on the molecular radius.

account for this difference and to enable a direct comparison, we have simulated frequency distributions for different NPC models and blockade modes. These simulations were based on concepts established previously (Peters et al., 1990; for details, see the section on Experimental Procedures) assuming that the k values of an assembly of membrane patches containing a single DC can be described, to a first approximation, by a normal distribution characterized by mean value k_1 and standard deviation σ_1. In patches containing more than one DC, the DCs are assumed to function independently of each other. Thus the mean k value of a membrane patch with n DCs is simply the product of n and k_1, and its standard deviation is the product of $\sqrt{n}$ and σ_1. To obtain the frequency distribution of k, the k distri-
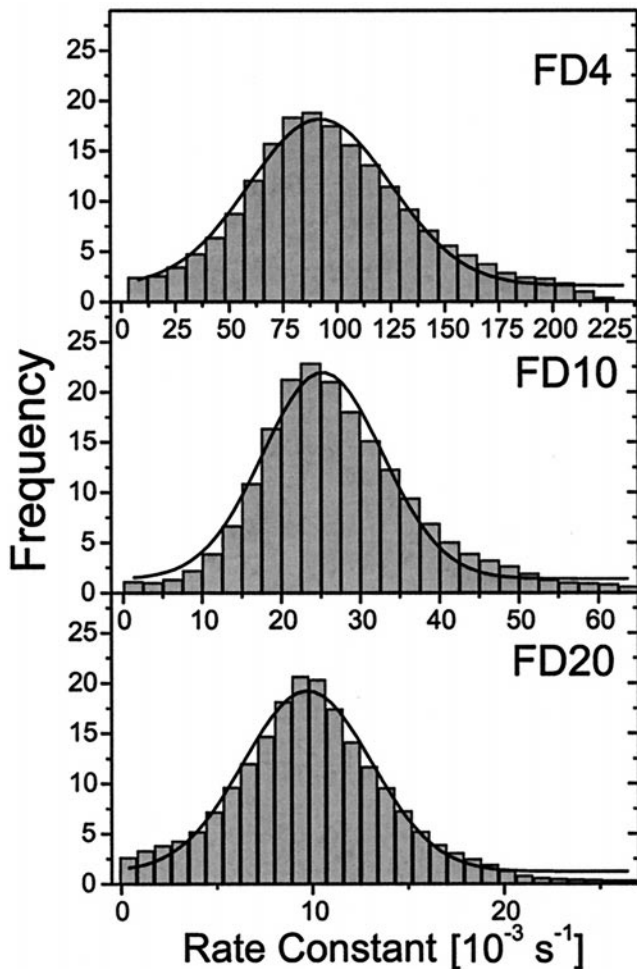
FIGURE 6 Results of measurements concerning large membrane patches. Employing a filter type with 1.8-μm-diameter filter pores to isolate membrane patches containing ~125 pore complexes for all probe molecules, a large number of OSTR measurements were made and the results were plotted as frequency diagrams. In all cases only a single peak was observed that could be fitted by a single Gaussian. The mean rate constant depended inversely on the molecular size of the probe, which is similar to the results obtained with filter pores of 0.18 μm diameter.

butions of patches with 0, 1, 2, . . . DCs are weighted by their probability density, i.e., the normalized distribution of n.

To perform simulations according to the described scheme, essentially four parameters have to be known or assumed: k_1, σ_0, σ_1', and the distribution of DCs among membrane patches. The above comparison of the experimental k distributions (Fig. 5) and the predicted DC distributions (Fig. 2) strongly suggested that the major peak of the experimental distributions is associated with membrane patches carrying a single DC. Therefore, we assign values to k_1, σ_0, and σ_1' on the basis of that peak and, restricting the discussion to the 10-kDa dextran, take k_1 as 19.8×10^{-3} s^{-1}, σ_0 as $\pm 3 \times 10^{-3}$ s^{-1}, and σ_1 as $\pm 5 \times 10^{-3}$ s^{-1}. The distributions of DCs among membrane patches shown in Fig. 2, a'-c'', were employed. Simulations based on these parameters are shown in Fig. 7.

Fig. 7, permitting a direct comparison of expectation and experiment, shows that the experimental data can be very well simulated, but only if computations are based on a single DC per NPC and the local blockade mode. If the computation is based on eight or nine DCs per NPC at local blockade mode (Fig. 7, b' and c'), the individual contributions of the patches with 5–20 DCs merge to yield a single, peculiarly shaped peak. All models assuming a global blockade mode (Fig. 7, a''-c'') yield only two well-spaced peaks, the predominant of which corresponds to $k = 0$, and the much smaller one to k_1 or k_8 or k_9. Thus the simulations again support the view that the NPC contains a single DC and that the local blockade mode is effective.

Independently of the above considerations, the comparison of transport measurements employing filters with pores of 0.18-μm diameter (Fig. 5) or 1.8-μm diameter (Fig. 6) supports the notion that the NPC contains a single DC. The relation between the rate constant k_1 obtained with small membrane patches containing few NPCs and the k_{125} obtained with large membrane patches containing many NPCs is given by Eq. 4. Insertion of pertinent values ($\sigma = 50$ NPC/μm^2, $A_{fp} = 0.025$ μm^2) yields $k_{125}/k_1 = 1.25$. The experimental values match this expectation quite well for the 10-kDa and 20-kDa dextrans ($k_{125}/k_1 = 1.27$ and 1.20), although, for reasons yet to be established, the k_{125}/k_1 ratio is 1.70 in the case of the 4-kDa dextran. If each NPC contained eight or nine DCs, the smaller membrane patches would already contain a considerable number of DCs, so that a k_{125}/k_1 value of 1.0 would be expected.

Determination of the dimensions of the diffusion channel

To a first approximation, transmembrane channels can be modeled as patent cylinders. The formalism for deriving the radius and length of the cylinder from permeability measurements was developed already in the early 1950s (Pappenheimer et al., 1951) and since then has been frequently applied (for review, see Renkin and Curry, 1979, Peters, 1986). Although based on macroscopic hydrodynamic principles and assuming, among other simplifications, that the probe molecules can be approximated as hard spheres, the approach has proved useful. It remains, however, a first approximation and should be considered as such.

The radius r_0 of a hollow cylinder with a passive permeability equivalent to that of the diffusion channel can be calculated according to Eq. 7 from the transport rate constant k_1, the diffusion coefficient D, and the Stokes radius a of two transport substrates. This procedure is based on the dependence of the transport rate constant on the molecular radius of the probe and thus does not require knowledge of the number of DCs per membrane patch or the length of the DCs. Therefore it can be applied to measurements corresponding to small or large membrane patches. In the present case r_0 values of 4.4–6.1 nm (mean 5.35 nm) were obtained, as listed in Table 2.

TABLE 1   Results of transport measurements

Probe	Mean molecular mass (kDa)	Diffusion coefficient* ($\mu m^2 \, s^{-1}$)	Stokes radius# (nm)	0.18-μm filter pores§								1.8-μm filter pores¶	
				n	f_0 (%)	k_1 ($10^{-3} \, s^{-1}$)	f_1 (%)	k_2 ($10^{-3} \, s^{-1}$)	f_2 (%)	k_3 ($10^{-3} \, s^{-1}$)	f_3 (%)	n	k ($10^{-3} \, s^{-1}$)
FD4	3.9	89.0	2.42	258	2	53.3	70	99.4	21	140.0	1	198	92.1
FD10	10.0	76.0	2.82	258	3	19.8	65	38.2	35			195	25.2
FD20	17.2	65.0	3.30	255	2	8.1	53	15.2	23	23.6	24	206	9.7

*Measured by fluorescence microphotolysis as described (Peters, 1984).
#Calculated according to $(kT)/(6\pi\eta D)$, where k = Boltzmann's constant, T = absolute temperature, and η = solvent viscosity.
§n, Number of measurements; f_0, f_1, f_2, f_3, fractions of membrane patches with no, one, two, or three NPCs, respectively, as determined by fitting Gaussians to the experimental data; k_1, k_2, k_3, mean transport rate constant of membrane patches with one, two, or three NPCs, respectively, as determined by fitting Gaussians to the experimental data.
¶n, Number of measurements; k, mean transport rate constant as determined by fitting a Gaussian to the experimental data.

Once r_0 has been determined, l_{DC} can be derived from k_1 for each probe molecule separately by employing Eq. 8. By these means we found (Table 2) that l_{DC} ranges from 40.8 to 49.8 nm (mean 44.5 nm). It may be pointed out that, in contrast to the determination of r_0, that of l_{DC} requires knowledge of k_1. Therefore l_{DC} could be determined for the first time in this study.

DISCUSSION

The NPC impresses the investigator as multitalented. It mediates both passive and signal-dependent transport. The latter is frequently unidirectional, but the direction may be either from cytoplasm to the nucleus or vice versa, depending on whether the substrate carries an import or export
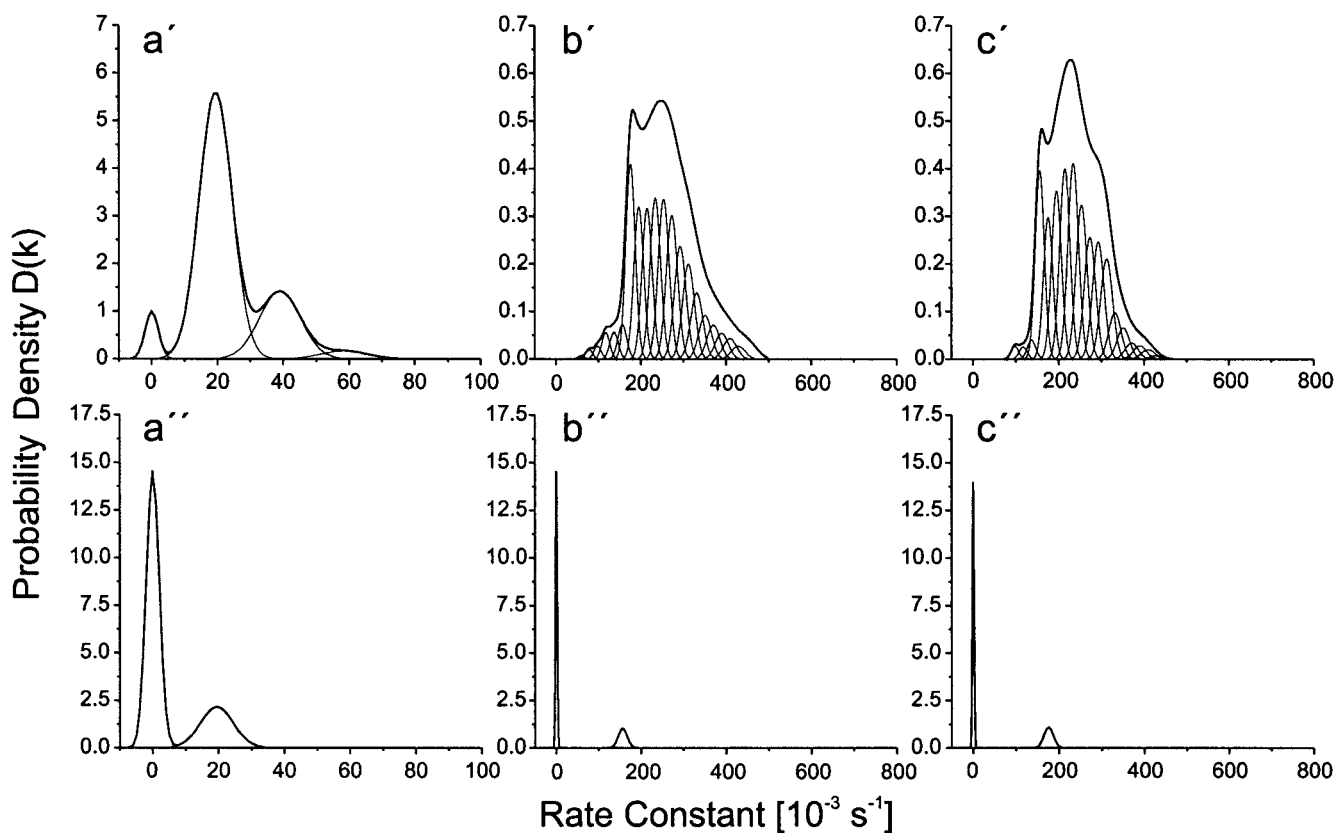

FIGURE 7   Simulation of nuclear pore complex models. Based on the models shown in Fig. 2 for the distribution of diffusion channels in the nuclear pore complex, the distributions of the transport rate constant that would correspond to the models were simulated (see text). Models assuming one, eight, or nine diffusion channels are considered in a, b, and c. a'–c' pertain to a situation in which the membrane-filter contact causes only a blockade of diffusion channels that are in direct contact (local blockade), and a''–c'' pertain to a situation in which a contact of NPC and filter induces the closing of all diffusion channels of that nuclear pore complex (global blockade). It can be recognized that only the assumption of a single diffusion channel per nuclear pore complex at local blockade is consistent with the experimental data (cf. Fig. 5). If the nuclear pore complex contains eight or nine diffusion channels at local blockade (b', c'), the contributions of the diffusion channels are closely spaced and cannot be resolved as individual peaks. For the case of a global blockade (a''–c''), a large fraction (~70%) of impermeable membrane patches is predicted for all three models, in contradiction to the experimental data (Fig. 5).

TABLE 2 Equivalent radius and length of the diffusion channel in the nuclear pore complex

Probe molecules	Equivalent radius (nm)	
	Derived from k_1	Derived from k_{125}
FD4 & FD10	5.0	4.4
FD4 & FD20	5.6	5.1
FD10 & FD20	6.1	5.9
Mean	5.35	
	Length (nm)	
FD4	43.0	
FD10	49.8	
FD20	40.8	
Mean	44.5	

signal. In addition, many substrates shuttle between cytoplasm and nucleus. In each transport direction there is a diversity of pathways, which at present are intensively studied.

For a while it appeared to be accepted that a common channel mediates all transport modes (Stevens and Swift, 1966; Paine et al., 1975). For instance, we estimated that in the living hepatocyte the number of patent diffusion channels amounts to ~60% of the number of NPCs, indicating that each NPC contains a channel for diffusion and transport, but that a fraction of the channels is temporarily plugged by molecules or particles in transit (Peters, 1984). However, one more recent structural study (Hinshaw et al., 1992) raised the possibility that the NPC contains, in addition to a pathway in the central granule for signal-dependent transport, a set of eight peripheral diffusion channels having an oval cross section with an average radius of 5.0 nm. Akey and Radermacher (1993) could not directly support the suggestion of Hinshaw et al. (1992), but found that the structure of the NPC leaves at best enough space for eight narrow peripheral slits with a radial diameter of 0–2 nm and circumferential dimensions of 19 nm. Strong evidence for a single central diffusion channel was provided by Feldherr and Akih (1997) showing that electron-dense particles of 4–7-nm diameter permeate the NPC through a single pathway located right in the NPC center.

In agreement with the results of Feldherr and Akin (1997), our data (Figs. 2, 5, and 7) clearly indicate that the NPC contains a single diffusion channel. The possibility that there are eight large peripheral channels, as suggested by Hinshaw et al. (1992), can be excluded. However, the presence of narrow, slit-like channels, as suggested by Akey and Radermacher (1993), cannot be ruled out. The smallest probe tested by us had a Stokes diameter of 4.8 nm and thus would not permeate through channels with a maximum width of 4 nm.

The equivalent radius of the diffusion channel in the NPC has been estimated previously for different cells, employing permeability measurements (Paine et al., 1975; Paine, 1975; Bonner, 1978; Peters, 1984; Lang et al., 1986), electrical conductance measurements (Reynolds and Tedeschi, 1984), or both (Paine, 1975). The values range between 3.4 and 6.5 nm. Thus the value reported in this study is consistent with previous studies. A closer look, however, discloses subtle differences. Paine et al. (1975) determined the equivalent radius of the diffusion channel of the NPC in the intact microinjected *Xenopus* oocyte to be 4.5 nm. Our present value of 5.35 nm pertains to the same cell type, but, to the isolated nucleus immersed in a plain buffer without any proteins added. This may indicate that the width of the channel is adjustable to a certain extent, depending on the environmental conditions.

The length of the diffusion channel, to the best of our knowledge, has not been determined before whereas assumptions about the length varied within wide limits. Paine et al. (1975), for instance, assumed a channel length of 15 nm. We employed a value of 30 nm (Peters, 1984). An upper limit for the channel length is provided by structural studies (Akey and Radermacher, 1993) giving the axial dimension of the central granule (transporter) as 62.5 nm. Thus our value of 44.5 nm suggests that the diffusion channel permeates the transporter but perhaps is funnel-shaped at one or both entrances.

A central aspect of the filter method for generating membrane patches is the tightness with which cell membranes are attached to isoporous filters. The membrane-filter seal has to be tight enough to prevent leakage of the transport substrate at the rim of the filter pores. In a previous study (Tschödrich-Rotter and Peters, 1998) we measured the permeability of single streptolysin O pores in erythrocyte membranes. Erythrocytes were attached to isoporous filters by a procedure similar to the one used in the present study, achieving, however, only a relatively loose seal. Thus membrane-filter contacts were impermeable for dextrans of ≥70 kDa only. A brief treatment with polyethylene glycol made the contacts somewhat tighter, i.e., impermeable for dextrans of ≥40 kDa. With the nuclear envelope we encountered a completely different situation. In this case the permeability of the membrane-filter contacts could be directly assessed only for probe molecules that cannot permeate through the diffusion channel of the NPC, e.g., dextrans of ≥40 kDa. However, the results reported for the transport of the 20-kDa, 10-kDa, and 4-kDa dextrans (Fig. 5) definitely imply that the membrane-filter seals were sufficiently tight for all probe molecules employed. If that had not been the case, the frequency diagrams would not have shown distinct maxima, but rather a single ill-defined maximum. Furthermore, other features of the frequency diagrams as well as the dependence of the transport rate constants on the molecular radii of the probes would not have been internally consistent.

Our present results imply that the NPC contains one central channel mediating both passive and signal-dependent transport. Therefore the different transport modes should strongly interfere with each other. We have started with measurements of signal-dependent import and export and their cross-talk. In the experiments conducted so far

(Keminer et al., 1999), recombinant proteins containing either a nuclear localization signal (import protein), a nuclear export signal (export protein), or no signal (control protein) served as transport substrates, and an extract of *Xenopus* eggs supplied all of the necessary soluble transport cofactors. We found, for instance, that the import protein was only imported, the export only exported, and the control protein not transported. Import and export depended on the addition of an ATP-regenerating system and could be inhibited by the lectin WGA. Transport rates, in terms of molecules per NPC per time, were consistent with rough estimates based on microinjection experiments involving living mammalian cells.

Together, our observations suggest that the methods employed by us for isolating the nuclear envelope of *Xenopus* oocytes and attaching it to isoporous filters do not disturb the function of the NPC. Therefore, and because of its numerous new properties, OSTR can be expected to open new avenues in the study of nucleocytoplasmic transport.

REFERENCES

Akey, C. W. 1995. Structural plasticity of the nuclear pore complex. *J. Mol. Biol.* 248:273–293.

Akey, C. W., and M. Radermacher. 1993. Architecture of the *Xenopus* nuclear pore complex revealed by three-dimensional cryo-electron microscopy. *J. Cell Biol.* 122:1–19.

Bean, C. P. 1972. The physics of porous membranes—neutral pores. *In* Membranes, Vol. 1. G. Eisenmann, editor. Dekker, New York. 1–54.

Bonner, W. M. 1978. Protein migration and accumulation in nuclei. *In* The Cell Nucleus, Vol. 6. H. Bush, editor. Academic Press, New York. 97–148.

Borer, R. A., C. F. Lehner, H. M. Eppenberger, and E. A. Nigg. 1989. Major nucleolar proteins shuttle between nucleus and cytoplasm. *Cell.* 56:379–390.

Cole, C. N., and C. M. Hamill. 1998. Nucleocytoplasmic transport: driving and directing transport. *Curr. Biol.* 8:R363–R372.

Dingwall, C., S. V. Sharnik, and R. A. Laskey. 1982. A polypeptide domain that specifies migration of nucleoplasmin into the nucleus. *Cell.* 30:449–458.

Evans, J. P., and B. K. Kay. 1991. Biochemical fractionation of oocytes. *Methods Cell Biol.* 36:133–148.

Feldherr, C. M., and D. Akin. 1997. The location of the transport gate in the nuclear pore complex. *J. Cell Sci.* 110:3065–3070.

Fischer, U., J. Huber, W. C. Boelens, I. W. Mattaj, and R. Lührmann. 1995. The HIV-1 rev activation domain is a nuclear export signal that accesses an export pathway is used by specific cellular RNAs. *Cell.* 82:475–483.

Franke, W. W., and U. Scheer. 1974. Structures and functions of the nuclear envelope. *In* The Cell Nucleus, Vol. 1. H. Bush, editor. Academic Press, New York. 219–347.

Goldstein, L. 1958. Localization of nucleus-specific protein as shown by transplantation experiments in *Amoeba proteus. Exp. Cell Res.* 15:635–637.

Görlich, D. 1998. Transport into and out of the cell nucleus. *EMBO J.* 17:2721–2727.

Hinshaw, J. E., B. O. Carragher, and R. A. Milligan. 1992. Architecture and design of the nuclear pore complex. *Cell.* 69:1133–1141.

Kalderon, D., W. D. Richardson, A. F. Markham, and A. E. Smith. 1984. Sequence requirements for nuclear localisation of SV40 large-T antigen. *Nature.* 311:33–38.

Keminer, O., J.-P. Siebrasse, K. Zerf, and R. Peters. 1999. Signal-dependent protein transport through single nuclear pores. *In* Proceedings of the European Congress on Cell Biology, Bologna, May 8–11, 1999 (Abstr.).

Lang, I., M. Scholz, and R. Peters. 1986. Molecular mobility and nucleo-cytoplasmic flux of macromolecules in hepatoma cells. *J. Cell Biol.* 102:1183–1190.

Maul, G. G. 1977. The nuclear and the cytoplasmic pore complex: structure, dynamics, distribution, and evolution. *Int. Rev. Cytol.* 6(Suppl.): 75–186.

Mattaj, I. W., and L. Englmeier. 1998. Nucleocytoplasmic transport: the soluble phase. *Annu. Rev. Biochem.* 67:265–306.

Meier, U. T., and G. Blobel. 1992. Nopp140 shuttles on tracks between nucleolus and cytoplasm. *Cell.* 70:127–138.

Melchior, F., and L. Gerace. 1995. Mechanism of nuclear protein import. *Curr. Opin. Cell Biol.* 7:310–318.

Michael, M., M. Choi, and G. Dreyfuss. 1995. A nuclear export signal in hnRNP A1: a signal-mediated, temperature-dependent nuclear export pathway. *Cell.* 83:415–422.

Moore, M. S., and G. Blobel. 1993. The two steps of nuclear import, targeting to the nuclear envelope and translocation through the nuclear pore, require different cytosolic factors. *Cell.* 69:939–950.

Nigg, E. A. 1997. Nucleocytoplasmic transport: signals, mechanisms and regulation. *Nature.* 386:779–787.

Paine, P. L. 1975. Nucleocytoplasmic movement of fluorescent tracers microinjected into living salivary gland cells. *J. Cell Biol.* 66:652–657.

Paine, P. L., L. C. Moore, and S. B. Horowitz. 1975. Nuclear envelope permeability. *Nature.* 254:109–114.

Paine, P. L., and P. Scherr. 1975. Drag coefficients for the movement of rigid spheres through liquid-filled cylindrical pores. *Biophys. J.* 15: 1087–1091.

Panté, N., and U. Aebi, 1996. Toward the molecular dissection of protein import into nuclei. *Curr. Opin. Cell Biol.* 8:397–406.

Pappenheimer, J. R., E. M. Renkin, and L. M. Borrero. 1951. Filtration, diffusion and molecular sieving through peripheral capillary membranes. *Am. J. Physiol.* 167:13–23.

Pemberton, L. F., G. Blobel, and J. S. Rosenblum. 1998. Transport routes through the nuclear pore complex. *Curr. Opin. Cell Biol.* 10:392–399.

Peters, R. 1983. Nuclear envelope permeability measured by fluorescence microphotolysis of single liver cell nuclei. *J. Biol. Chem.* 258:11427–11429.

Peters, R. 1984. Nucleo-cytoplasmic flux and intracellular mobility in single hepatocytes measured by fluorescence microphotolysis. *EMBO J.* 3:1831–1836.

Peters, R. 1986. Fluorescence microphotolysis to measure nucleocytoplasmic transport and intracellular mobility. *Biochim. Biophys. Acta.* 864: 305–359.

Peters, R., J. Peters, K. H. Tews, and W. Bähr. 1974. A microfluorimetric study of translational diffusion in erythrocyte membranes. *Biochim. Biophys. Acta.* 367:282–294.

Peters, R., H. Sauer, J. Tschopp, and G. Fritzsch. 1990. Transients of perforin pore formation observed by fluorescence microscopic single channel recording. *EMBO J.* 9:2447–2451.

Reichelt, R., A. Holzenburg, E. L. Buhl, Jr., M. Jarnik, A. Engel, and U. Aebi. 1990. Correlation between structure and mass distribution of the nuclear pore complex and of distinct pore complex components. *J. Cell Biol.* 110:883–894.

Renkin, E. M., and F. E. Curry. 1979. Transport of water and solutes across capillary endothelium. *In* Transport Organs. G. Giebisch, editor. Springer-Verlag, Heidelberg. 1–45.

Reynolds, C. R., and H. Tedeschi. 1984. Permeability properties of mammalian cell nuclei in living cells and in vitro. *J. Cell Sci.* 70:197–207.

Smith, I. D., X. Weilong, and R. L. Varnold. 1991. Oogenesis and oocyte isolation. *Methods Cell Biol.* 36:45–60.

Stevens, B. J., and H. Swift. 1966. RNA transport from nucleus to cytoplasm in *Chironomus* salivary glands. *J. Cell Biol.* 31:55–66.

Tschödrich-Rotter, M., U. Kubitscheck, G. Ugochuckwu, J. Th. Buckley, and R. Peters. 1996. Optical single-channel analysis of the aerolysin pore in erythrocyte membranes. *Biophys. J.* 70:723–732.

Tschödrich-Rotter, M., and R. Peters. 1998. An optical method for recording the activity of single transporters in membrane patches. *J. Microsc.* 192:114–125.

Wedekind, P., U. Kubitscheck, O. Heinrich, and R. Peters. 1996. Line-scanning microphotolysis for diffraction-limited measrements of lateral diffusion. *Biophys. J.* 71:1621–1632.

Wedekind, P., U. Kubitscheck, and R. Peters. 1994. Scanning microphotolysis: a new photobleaching method based on fast intensity modulation and confocal imaging. *J. Microsc.* 176:23–22.

Wen, W., J. L. Meinkoth, R. Y. Tsien, and S. S. Taylor. 1995. Identification of a signal for rapid export of proteins from the nucleus. *Cell.* 82:463–473.